
Spreads in Effective Learning Rates: The Perils of Batch Normalization During Early Training

Christian H.X. Ali Mehmeti-Göpel
Department of Computer Science
Johannes-Gutenberg University Mainz
chalimeh@uni-mainz.de

Michael Wand
Department of Computer Science
Johannes-Gutenberg University Mainz
wandm@uni-mainz.de

Abstract

Excursions in gradient magnitude pose a persistent challenge when training deep networks. In this paper, we study the early training phases of deep normalized ReLU networks, accounting for the induced scale invariance by examining effective learning rates (LRs). Starting with the well-known fact that batch normalization (BN) leads to exponentially exploding gradients at initialization, we develop an ODE-based model to describe early training dynamics. Our model predicts that in the gradient flow, effective LRs will eventually equalize, aligning with empirical findings on warm-up training. Using large LRs is analogous to applying an explicit solver to a stiff non-linear ODE, causing overshooting and vanishing gradients in lower layers after the first step. Achieving overall balance demands careful tuning of LRs, depth, and (optionally) momentum. Our model predicts the formation of spreads in effective LRs, consistent with empirical measurements. Moreover, we observe that large spreads in effective LRs result in training issues concerning accuracy, indicating the importance of controlling these dynamics. To further support a causal relationship, we implement a simple scheduling scheme prescribing uniform effective LRs across layers and confirm accuracy benefits.

1 Introduction

Since the rise of modern deep learning with AlexNet [Krizhevsky et al., 2012] in 2012, the trend towards deeper and bigger models is steady, culminating recently in (very) large language models such as GPT-4 [OpenAI, 2023]. Network depth seems to be a crucial factor, since along with its width, it upper bounds expressivity [Bartlett et al., 2019]. Empirically, deeper networks tend to enhance performance [Tan and Le, 2019], but with diminishing returns for large increases. Early models such as VGG-16 [Simonyan and Zisserman, 2015] suffer from instabilities such as vanishing [Hochreiter, 1991], exploding [Zhang et al., 2019] and shattering [Balduzzi et al., 2017] gradients, preventing researchers from building very deep models. Since then, many techniques claiming to alleviate said problems have been developed and utilized. Arguably, the two most notable ones are Residual Connections [He et al., 2016a] and Batch Normalization [Ioffe and Szegedy, 2015], which are ubiquitous in modern neural network architectures. Our paper focuses on the latter.

Understanding of the benefits of BatchNorm is not straightforward and still subject to debate. The initial claim that it increases trainability because it reduces internal covariate shift was quickly refuted [Awais et al., 2021] and many alternative explanations were proposed, such as smoothing of the loss surface [Santurkar et al., 2018] or enabling bigger learning rates [Bjorck et al., 2018]. Interestingly, while batch normalization keeps the propagated features at a constant magnitude (expected variance), it leads to exploding gradients in lower layers at initialization [Yang et al., 2019a] due to difference in how gradients and features propagate. Lubana et al. [2021] propose a unified framework that analyzes the benefits of regularization layers such as stable forward and backward propagation.

Empirically, placement of BatchNorm layers has significant impact in deep CNNs [Hasani and Khotanlou, 2019], as well as for Transformer architectures [Vaswani et al., 2017]. Moving LayerNorm *after* each sublayer’s residual connection yields significant improvements in convergence speed and robustness [Vaswani et al., 2018], as does the more recent “NormFormer” architecture [Shleifer et al., 2021] which adds normalization layers to the feedforward blocks. This in particular increases stability at higher learning rates by bringing measured average gradient norms closer across layers. Notably, gradient norms initially diverge significantly but converge after a few optimization steps. Our paper explains this effect, as well as similar observations for CNNs and other architectures, by a modeling the dynamic changes of relative effective learning rates that occurs when normalization layers are placed correctly and a suitable training protocol is used.

2 Related Work and Contributions

Salimans and Kingma [2016] introduced WeightNorm, a method to decouple a layer’s length and direction by training them as independent network parameters. They also demonstrated that in weight-normalized networks, gradients are orthogonal to layer weights, allowing update size calculation via the Pythagorean theorem. Hoffer et al. [2018] showed that the "effective step size" in normalized networks is approximately proportional to $\frac{1}{\|W\|_2}$ and proposed constraining it by normalizing layer weights. They further argued that the benefit of weight decay can be reduced to learning rate scheduling in normalized networks. Arora et al. [2019] described the auto rate-tuning effect, proving asymptotic convergence to a stationary point without manual tuning of learning rates for specific layers, given certain assumptions.

These results leave one important question unexplored: How do these layer-wise effects affect the ratio of learning speeds across different layers? We first define a layer’s *effective learning rate* (ELR) as the ratio of gradient-to-weight norms, accounting for scale invariance in normalized networks. Assuming constant gradient magnitude per layer during initial training steps, we developed a model predicting the dynamics of layerwise ELR evolution in early training. In the gradient flow, this behavior reduces to a non-linear ODE with a closed-form solution, where ELR spread vanishes over time. For larger λ , the behavior changes due to overshooting, and ELRs do not converge. Our model also reveals that warm-up learning rate schedulers, residual connections, and, under stronger assumptions, momentum [Botev et al., 2017] can help lowering the ELR spread.

Through CV and NLP experiments, we demonstrate that our model’s qualitative predictions for ELR mean and spread hold true in real training scenarios with varying learning rate, momentum and warm-up configurations. We also find a correlation between high ELR spreads and low trainability in different settings. Lastly, we give constructive evidence linking low ELR spreads to increased trainability by re-scaling gradients, especially in scenarios with a high spreads (e.g. without residual connections or warm-up phase). This approach is similar to the one of Hoffer et al. [2018] that constrains the layerwise weight norms to a constant, but avoids repeatedly exploding gradients by constraining gradients directly before applying them. This is consistent with the authors reporting stability issues when using WeightNorm alongside BatchNorm and resorting to mean-only BatchNorm. Our method allows us to constrain the ELR in a (full) BatchNorm setting, retaining a stable forward pass and other benefits of BatchNorm mentioned in the introduction.

3 General Auto Rate-Tuning Effect and Its Dynamics

The core observation is that for any layer N that is invariant to scaling in the forward pass $N(\gamma \cdot x) = N(x)$ (e.g. all normalization layers), its gradient scales inversely with its input:

$$\frac{dN}{d\gamma x}(\gamma x) = \frac{1}{\gamma} \frac{dN}{dx}(x). \tag{1}$$

This has been shown for BatchNorm by Wu et al. [2018] and for LayerNorm by Xiong et al. [2020]. Secondly, Arora et al. [2019] show that since normalization layers are scale invariant, no gradient can flow in this direction. Hence, weight updates ∇W are orthogonal to the weights W themselves:

$$\langle \nabla W, W \rangle = 0. \tag{2}$$

We now explore how this affect the early training dynamics of gradient magnitudes $\|\nabla W\|_F$ and effective gradient magnitudes $\|\nabla W\|_F/\|W\|_F$. Intuitively, the weight norm of layers with high

gradient norms grows fast and thus downscales the gradient, leading to auto-regulation: this effect is called *auto rate-tuning*.

3.1 Training Dynamics Induced by Auto Rate-Tuning

To model training dynamics, we assume that weights of a given layer, as well as their gradients, are random matrices where entries are normally distributed with zero mean and a time-dependent standard deviation that is uniform in each layer. We measure training time $t \in \mathbb{R}$ in the sense of $t = k\lambda$ after k optimization steps. In this notation, gradient descent updates can be written as $W(t + \lambda) = W(t) - \lambda \nabla W(t)$. The updates preserve zero norm and uniform variance of all entries in $W(T)$. Assuming full mutual independence of all entries in the weight and gradient matrices, we can deduce the following update rule from the orthogonality condition (2):

$$\|W(t + \lambda)\|_F^2 = \|W(t)\|_F^2 + \lambda^2 \|\nabla W(t)\|_F^2. \quad (3)$$

Condition (1) implies that gradient updates are inversely proportional to the current layer weights. If we assume that the "base gradient" for a layer is approximately constant for the first few steps of training, we therefore obtain (using shorthand $\sigma^2(t) := \|W(t)\|_F^2$ for simplicity)

$$\sigma^2(t + \lambda) = \sigma^2(t) + \frac{\lambda^2 c^2}{\sigma^2(t)} \quad (4)$$

for a constant initial gradient magnitude c depending only on layer depth. We call this the **discrete model**. We will now see that for an infinitesimal learning rate, we can resolve this recurrence analytically and obtain a closed solution. Solving for the difference quotient, we obtain:

$$\frac{\sigma^2(t + \lambda) - \sigma^2(t)}{\lambda} = \frac{\lambda c^2}{\sigma(t)^2} \quad (5)$$

In the limit $\lambda \rightarrow 0$, this yields the gradient flow that can be expressed as a nonlinear first order differential equation :

$$\frac{d\sigma^2}{dt} = \frac{\lambda c^2}{\sigma^2} \quad (6)$$

We will further call this the **continuous model**. The exact positive solution to the differential equation is given by:

$$\sigma^2(t) = \sqrt{2\lambda c^2 t + k_0}. \quad (7)$$

Assuming He initialization [He et al., 2015], the expected initial squared weight norm is 2 for layer width n . Thus, $2 = \sigma^2(0) = \sqrt{k_0}$, i.e., $k_0 = 4$.

3.2 Auto Rate-Tuning Affects Each Layer Separately

The dynamic re-scaling of gradients explored above applies to each layer independently and does not affect layers above or below. We consider a simple concatenation of a linear layer $L(x, \gamma W) = x^T(\gamma W)$ followed by a normalization layer N . If we derive the output of N with regard to the layer's weights, we obtain by the chain rule:

$$\frac{dN}{d\gamma W}(x, \gamma W) = \frac{1}{\gamma} \frac{dN}{dL}(x, W) \cdot \frac{dL}{dW}(x, W) = \frac{1}{\gamma} \frac{dN}{dW}(x, W).$$

On the other hand, if we derive with regard to the input x , the extra factor $\frac{1}{\gamma}$ cancels out :

$$\frac{dN}{dx}(x, \gamma W) = \frac{1}{\gamma} \frac{dN}{dL}(x, W) \cdot \gamma \frac{dL}{dW}(x, W) = \frac{dN}{dW}(x, W).$$

This implies that if we want to simply model auto rate-tuning effects in the network, a simple layer-wise view is sufficient.

3.3 Assumptions on Initial Gradient Norm

Feed-forward networks: The dynamics of Eq. 7 apply to all normalized layers equally, but the initial gradient norms $c_\ell = \|\nabla W_\ell(0)\|_F$ differ substantially across layers $\ell = 1 \dots L$: Yang et al. [2019b] show that in feedforward networks with Batch Normalization, the gradient norm at initialization grows as:

$$\|\nabla W_\ell(0)\|_F^2 \sim \alpha^{L-\ell+o(\ell)}, \quad (8)$$

with $\alpha = \sqrt{\pi/(\pi-1)} \approx 1.21$ (see also [Luther, 2020] for a simplified derivation).

ResNets: When considering residual networks, skip-connections dampen exploding gradients by exponential down-weighting [Ali Mehmeti-Göpel et al., 2021]. Assuming additivity of variances, we can compute the initial gradient magnitudes in a ResNet with the following recursion:

$$\|\nabla W_\ell\|_F(0) = \begin{cases} \frac{1}{2}(\alpha \cdot \|\nabla W_{\ell+1}\|_F(0) + \|\nabla W_{\ell+s}\|_F(0)) & \text{if } \ell \equiv 0 \pmod{s} \text{ and } \ell < L - s \\ \alpha \cdot \|\nabla W_{\ell+1}\|_F(0) & \text{otherwise,} \end{cases} \quad (9)$$

where the base case is $\|\nabla W_L\|_F(0) = \alpha$, and s represents the number of layers a residual connections skips. This formula averages the contribution from the main and residual branch since the residual connection is usually followed by a normalization layer or a linear layer followed by a normalization layer, effectively halving the contributions from the main and residual branch.

3.4 Asymptotic Behavior of Effective Learning Rates

Accounting for scale invariance of normalized networks, we define the *effective learning rate* of a layer as $E(t) := \frac{\|\nabla W\|_F(t)}{\|W\|_F(t)}$, as it relates to the relative distance moved in weight space. We consider the ratio of effective learning rates between two layers l and k in our continuous model:

$$\mathbb{E} \left(\frac{E_\ell^2}{E_k^2} \right) (t) = \frac{c_\ell^2}{(\sigma_\ell^2(t))^2} \cdot \frac{(\sigma_k^2(t))^2}{c_k^2} = \frac{c_\ell^2(2\lambda c_k^2 t + k_0)}{c_k^2(2\lambda c_\ell^2 t + k_0)} \xrightarrow{t \rightarrow \infty} 1 \quad (10)$$

This result suggest that (according to our model) BatchNorm will equalize effective learning rates perfectly over time, even through it starts with exploding gradients. We show in the appendix that this is often not the case practice: Realizing this behavior is non-trivial, as we have to deal with discrete time steps. In our simulation and experiments, we will refer to $Std(E_k)$ over all layers k in the network as the *effective learning rate spread* of the network.

3.5 Discrete Behavior

The second key insight in our paper, complementing the continuous model in Eq. 7, is that the we might obtain quite different solutions for finite (larger) numerical steps λ . As detailed in the appendix, the ODE in Eq. 6 is a stiff non-linear equation: the derivative of the right hand side by the variance $\sigma^2(t)$ is $a = -\lambda \cdot c_\ell^2 / [\sigma^2(t)]^2$, which is worst for $t = 0$. In order to solve the equation stably, we have to use an initial step width of $\lambda \ll 2\sqrt{2}(\alpha^{-L})$.

Large, fixed step sizes: If we train normalized networks with (realistically) large, steps, our model predicts weight norms to overshoot, leading to *vanishing* gradients at layers of initially large gradient magnitude, again leading to frozen layers for large L .

Warm-up solves the convergence issue by growing the step sizes (very) quickly while staying within the stability range (see appendix).

Our experiments in Section 4 confirm these predictions wrt. to all of these three training regimes.

3.6 Placement of Normalization Layers

As already noted by Arora et al. [2019], a necessary condition for auto rate-tuning of a layer is its scale-invariance. Being based on the same mechanism, this extends naturally to the tuning of ELR-ratios. Note that multiple linear layers followed by a normalization layer should be auto-rate tuned since they remain scale-invariant. ReLU or Leaky ReLU layers between the linear layer and the normalization layer do not break the auto rate-tuning property either, since they are positive homogeneous functions. If a residual connection is placed in-between a linear layer and the corresponding normalization layer,

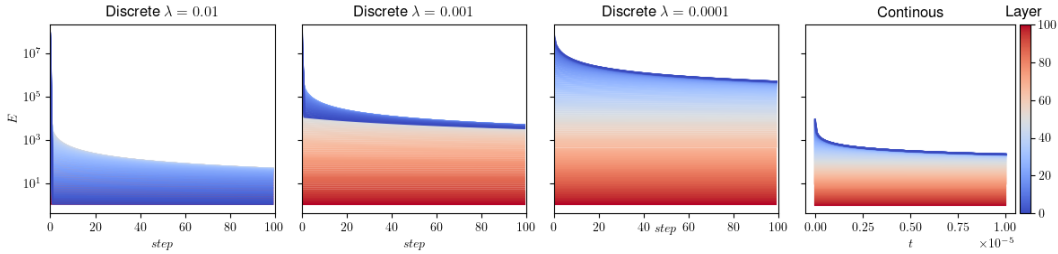


Figure 1: Comparing the evolution of the layerwise simulated effective learning rate for different values of λ in the discrete and the continuous model.

it can break auto rate-tuning; note that this is the case in a ResNet v2 [He et al., 2016b]. A sufficient condition for scale-invariance and thus auto rate-tuning is adding a normalization layer directly after every linear layer, potentially explaining improvements in NormFormers [Shleifer et al., 2021].

4 Simulations and Experimental Validation

In the following, we compare predictions by our discrete model with empirical measurements. We chose ResNet v1 [He et al., 2016a] with ("Short") and without ("NoShort") residual connections as well as a Transformer Vaswani et al. [2017] as examples of standard architectures. We chose a ResNet v1 as opposed to a v2 since in the former, the "correct" placement of normalization layers (ref. Section 3.6) is given without modifying the architecture. Theory predicts that a high number of layers and not using residual connections increase the strength of the observed effect (ref. Section 3.3). We therefore use 56 and 110 layer networks: Without residual connections, the former is deep but still trainable and the latter is mostly untrainable with regular protocols.

For computer vision tasks, we work with standard image classification datasets of variable difficulty: CIFAR-10, CIFAR-100 [Krizhevsky, 2009], CINIC-10 Darlow et al. [2018] and ILSVRC 2012 (called ImageNet in the following) [Deng et al., 2009]. As for NLP tasks, we use the Multi30k Elliott et al. [2016] machine translation task (German to English).

For optimizers, we mostly compare three different basic setups: (1) SGD with momentum and weight decay with hand-tuned hyper-parameters (2) SGD without momentum or weight decay (3) SGD without momentum or weight decay, where we constrain the effective learning rate of each layer as explained below. We further use different kinds of learning rate scheduling with and without warm-up; further details about the architectures and training process can be found in the supplementary material.

4.1 The Effect of Higher Learning Rates: Discrete Model vs Continuous Model

In Figure 1, we simulate the evolution of layerwise ELRs for different learning rates in the discrete and the continuous model. As initial conditions, we chose $\|W_\ell\|_F(0) = 1$ for all layers $\ell = 0 \dots L - 1$ and c_ℓ growing exponentially for $\ell \rightarrow 0$, imitating exploding gradients at initialization as discussed in Section 3.3. We show only a single learning rate for the continuous model, as changing the learning rate merely re-scales the solution. We see that for very low learning rates, the behavior of the discrete model indeed looks qualitatively very similar to the continuous model. For higher learning rates, the behavior of the discrete and continuous model starts to differ: the ELR of layers with very high initial ELR "flips" below layers that have a lower initial ELR, after only one step. This occurs due to initial gradient explosion, leading to a substantial increase in their weight norm in the first step, which in turn results in an extremely low effective learning rate in the subsequent step. This behavior lies in the discrete nature of the model and cannot be explained by the continuous model, as the function $\sigma^2(t)$ is monotonous in c , the parameter that is determined by the initial gradient norm.

4.2 Relationship Between Effective Learning Rate and Learning Rate

Because of the effect of discretization explained in Section 4.1, the relationship the learning rate λ chosen as a hyper-parameter the resulting effective learning rate of a network is non-trivial. We ran a simulation of our discrete model with 56 layers for a range of learning rates, for 10 steps initialized to emulate a network with and without skip-connections. In Figure 2, we show the average and spread

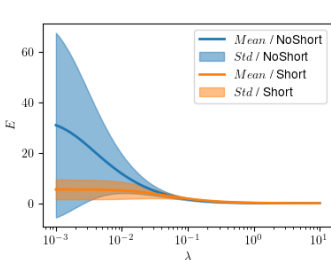


Figure 2: **Simulated** ELR mean/spread after 10 steps in our discrete model for different values of λ .

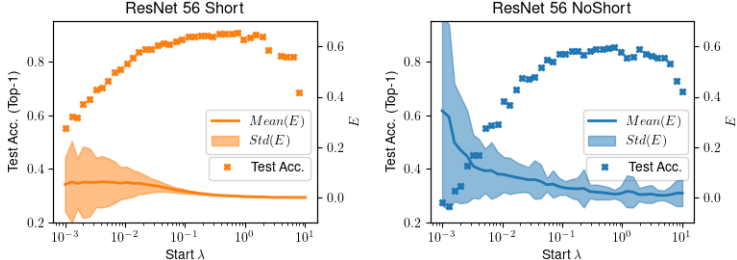


Figure 3: **Real** test performance, ELR mean and spread of a ResNet56 Short/NoShort training on Cifar10 for different values of λ . ELR values are averaged over the whole run.

of the effective learning rate calculated over all layers in the last step. We chose to only plot the statistics of the 10th step, since most of the movement should and seems to be happening in the first steps and we conjecture running as few as 10 steps might be enough to make qualitative predictions for real networks. Interestingly we see that both $Mean(E)$ and $Std(E)$ decrease for increasing λ and that the effect is more pronounced on the networks without skip-connections. Revisiting Figure 1, this makes sense: due to the discretization dynamic, both the average and spread of the ELR are visibly lower for higher learning rates after a few steps.

To confirm our predictions, we trained a ResNet56 Short/NoShort on Cifar10 for multiple initial learning rates, measured the average and spread of the effective learning rate averaged over the entire training process. Note that we only compare qualitative behavior between simulation and reality, as the exact values for initial weight and gradient norm differ from the real network to our simulation. In Figure 3, we see that qualitatively, the predictions are confirmed: for learning rates lower than $\approx 10^{-1}$, the ELR spread start to increase. Note that the measured high spreads for low λ do not contradict the results from Section 3.4, as the time needed for the ELRs to equalize is impracticably high because of the exponential disparity in initial conditions due to exploding gradients. This effect is stronger for NoShort networks than for Short networks. Additionally, we can see that a very high spread in ELR seems to correlate with low test accuracies.

4.3 Effects of Momentum on Auto Rate-Tuning

Momentum SGD methods originally introduced by Polyak [1964] remain consistently used by deep learning practitioners over the last years. As momentum fundamentally impacts the evolution of gradient magnitudes over time, we expect to see an impact on the evolution of effective learning rates. Integrating the momentum formula:

$$\nabla W(t) = \mu \cdot \nabla W(t - \lambda) + \nabla \widehat{W}(t), \quad (11)$$

where $\nabla \widehat{W}$ is the "base gradient" and ∇W is the gradient after applying the momentum formula to our model. Its computation is not straightforward, because since the gradients accumulate, some assumptions on the relative gradient angles have to be made. We additionally assume that all base gradients $\widehat{\nabla} W(t)$ are random i.i.d. vectors and thus orthogonal to each other with high likelihood. This allows for an orthogonal decomposition of $\nabla W(t)$, and yields for discrete $t = k \cdot \lambda$:

$$\|\nabla W(k\lambda)\|_F^2 = \sum_{i=0}^k \mu^{2(n-i)} \cdot \|\nabla \widehat{W}(i\lambda)\|_F^2 \quad (12)$$

$$\|W((k+1)\lambda)\|_F^2 = \|W(0)\|_F^2 + \lambda^2 \sum_{j=0}^k \left(\frac{1 - \mu^{k+1-j}}{1 - \mu} \right)^2 \|\nabla \widehat{W}(j\lambda)\|_F^2. \quad (13)$$

We believe that the i.i.d. random/orthogonality assumption can be a reasonable approximation at least for larger learning rates. The details of the derivation can be found in the appendix. Using this model, we computed the ELR spread after 50 steps for a 56-layer network for different values of μ and λ in Figure 4. We chose 50 steps as it takes a number of steps for momentum to impact ELR

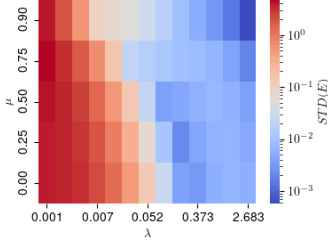


Figure 4: **Simulated** ELR spread after 50 steps in our discrete model for different values of λ and μ .

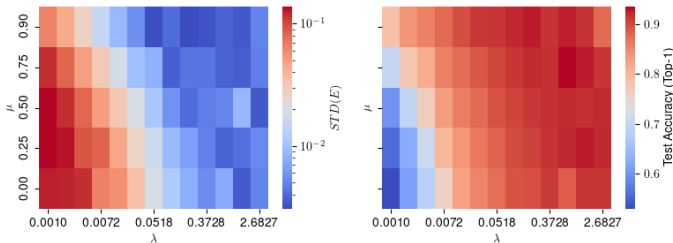


Figure 5: **Real** ELR spread and test performance in a ResNet56 Short training on Cifar10 for different values of λ and μ . ELR values are averaged over the whole run.

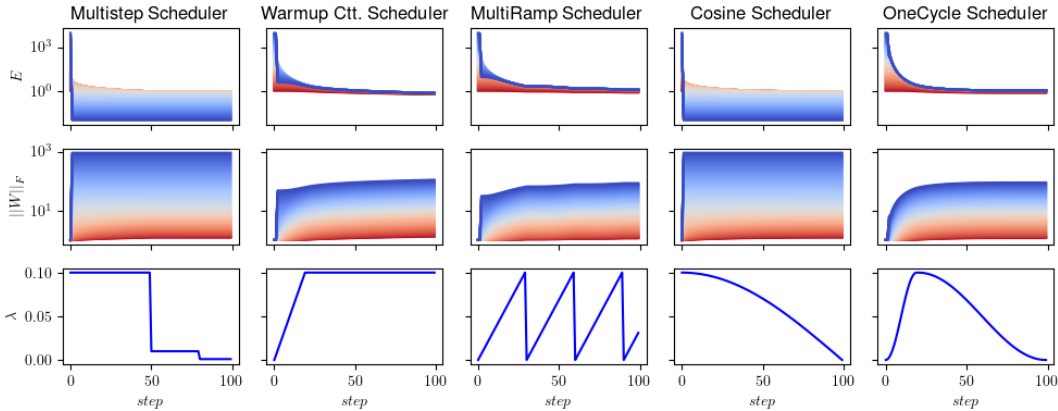


Figure 6: Simulated evolution of layerwise ELRs and weight norms for popular LR schedulers.

spread, especially for small learning rates. Plots for different amount of steps look similar and can be found in the appendix. We see that overall, using momentum seems to lower the effective learning rate spread. Only for very small values of λ the effect is not clear, a regime where our assumptions are unrealistic.

To confirm our predictions, we trained a ResNet56 Short on Cifar10 for multiple values of λ and μ and show the measured ELR spread averaged over the entire training process. In Figure 3, we see that for small and medium learning rates, high values for μ result in a smaller ELR spread. Networks with a very high ELR spread (low μ and λ) do indeed seem to train badly and raising μ seems indeed to result in a higher test accuracy for those networks. Overall, the predicted behavior the ELR spread seems to qualitatively match reality.

4.4 Effects of Warm-Up on Auto Rate-Tuning

Our model is effortlessly extends to a scenario where learning rates change over time. In Figure 6, we simulated the evolution of the effective learning rates and weight norms for popular learning rates schedulers with our discrete model. We see that all methods involving a gradual increase of the learning rate (warm-up) result in a reduction in ELR spread. This is in-line with our theoretical results in Section 3.4, predicting that the dynamics are closer to our continuous model for small learning rates λ , where effective learning rates converge over time.

To confirm our predictions, we trained a ResNet10 Short on Cifar10 for 50 epochs using a simple cosine scheduler (no warm-up, strictly decaying λ) and a OneCycle scheduler (includes a warm-up phase) with the same peak LR. As the reported main benefit of OneCycle schedulers lies in reaching a acceptable accuracy in a very short time, we chose a harder dataset and a low number of epochs. We train the basic three setups as described at the beginning of this section, each with and without warm-up. In Figure 7, we report results averaged over 5 runs (shades indicate the standard deviation): the validation accuracies and mean values for $\lambda \cdot E$ averaged over the entire training run. As the

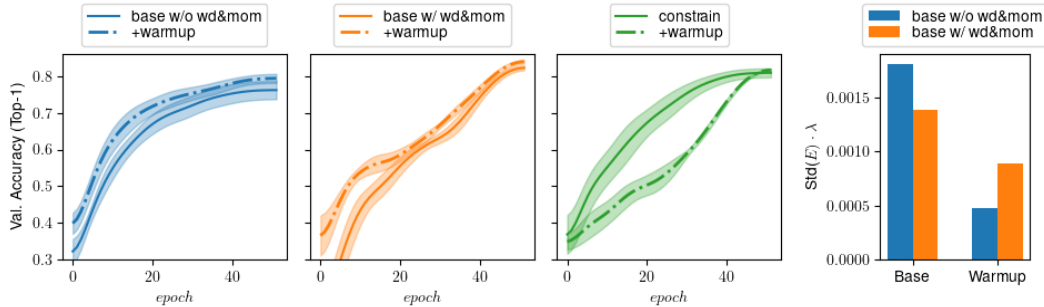


Figure 7: Validation accuracy (line plots) and mean ELR spread (bar plot) of a ResNet110 Short trained on Cinic10 for 50 Ep. with and without learning rate warm-up averaged over 5 different runs.

learning rate over time is different over the chosen setups, it is imperative to compare the values of $\lambda \cdot E$ instead of the plain effective learning rate to accurately compare the statistics. We see that warm-up consistently lowers the average weighted ELR spread for both regular training runs which results in faster training and higher final accuracies.

4.5 Constraining the Effective Learning Rate

In the past sections we came to understand that according to our model, we can control the effective learning rate of the layers in many ways: by controlling the magnitude of weights, the magnitude of gradients, or by scheduling the learning rate. In theory, these variants may be equivalent but in very deep networks without residual connections, as the gradient norm grows exponentially in the amount of layers, we want to limit the magnitude of the first gradient before it even gets applied in order to avoid "breaking" the network to the point of numerical instability. We therefore resort to normalizing the layerwise gradients ∇W by the effective learning rate before applying the gradients to the weights in the optimizer step:

$$\nabla W \leftarrow \nabla W \cdot \frac{E_{goal}}{E + \epsilon}, \quad (14)$$

for a given constant goal effective learning rate E_{goal} and a small ϵ we chose as $\epsilon = 10^{-5}$. In a basic setting without weight decay, this would lead to strictly increasing weight norms W over the course of the training. This can lead to instability for higher values of E_{goal} . To remedy this problem, we additionally divide all layer weights by the maximum layer weight $\widehat{W} = \max(\|W\|_F)$ over all layers before every step. This should not change the network function since normalization layers are scale invariant and gradients are normalized. It is important to also update the "running mean" value μ of a Normalization layer so the computations are still correct at validation time: $W \leftarrow \frac{W}{\widehat{W}}, \quad \mu \leftarrow \frac{\mu}{\widehat{W}}$.

4.6 Training and Performance of Constrained ELR Training

Going back to Figure 7 we observe that as expected, unlike the regular training runs, warm-up doesn't result in an increased accuracy when using our ELR-constrain method. This supports our claim that one of the benefits of warm-up lies in reducing ELR spreads.

We show the test performance of a ResNet110 Short/NoShort trained on Cifar10 for multiple initial learning rates, using the three basic setups described at the beginning of the section. In Figure 8, we see that for "Short" networks with the respective best (effective) learning rate, our method significantly outperforms the basic training without weight decay and momentum and even slightly outperforms the basic training with handcrafted values for weight decay and momentum. For the networks without skip-connections, we are able to train to a maximum of 73.9% whereas the best network using conventional training performs with 34.0%, a significant difference. In the appendix, we show similar results for Cifar100, with the difference that our method's top accuracy is slightly lower than the best run for basic training with momentum and weight decay but still significantly better than the runs without.

In Figure 9, we trained a ResNet101 NoShort for 50 epochs on ImageNet, comparing our three usual

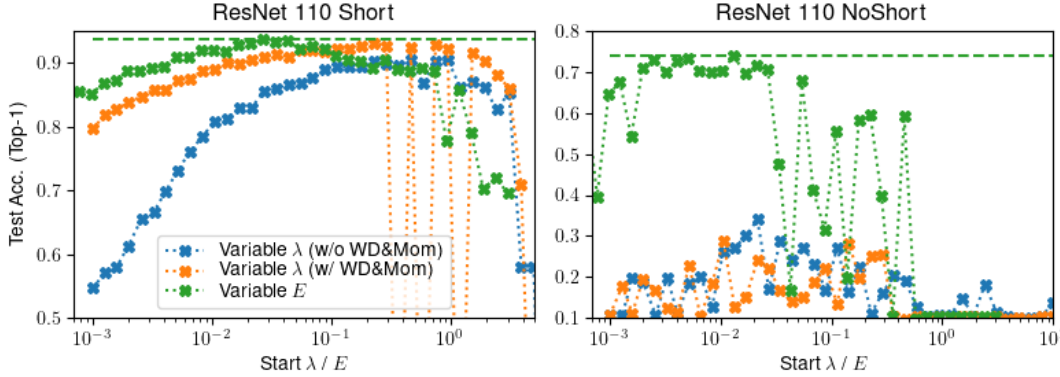


Figure 8: Test accuracy of a ResNet110 Short/NoShort trained on Cifar10 for different initial λ (regular training) or E (constrained ELR training). The dashed line indicates the top accuracy reached.

Constrain	Wd. & Mom.	Warmup	Test Acc. (Top-1)	$Std(E) \cdot \lambda$
No	Yes	Yes	78.1%	$3.310 \cdot 10^{-4}$
No	Yes	No	77.3%	$3.958 \cdot 10^{-3}$
No	No	Yes	74.5%	$4.903 \cdot 10^{-5}$
No	No	No	73.1%	$5.117 \cdot 10^{-3}$
Yes ($E_{goal} = 0.006$)	No	Yes	76.9%	-
Yes ($E_{goal} = 0.006$)	No	No	74.1%	-
Yes ($E_{goal} = 0.01$)	No	No	75.2%	-

Figure 9: Performance of a Resnet110 Short on ImageNet in different settings.

setups with (OneCycle scheduler) and without warm-up (cosine scheduler) to our ELR constrain method. We see that warm-up lowers the spreads and results in better accuracies. We can also confirm that our method is usable on bigger datasets, a setting where WeightNorm is reportedly unstable. For the hyper-parameters chosen, basic training with warmup, momentum and wd. outperforms our method, but an expensive hyper-parameter sweep over λ and E_{goal} would be necessary to assuredly assert which method performs best.

In the appendix, we show a similar experiment involving Transformer architectures on a NLP task. In the chosen setup, the network tends to diverge during early training without warm-up. However, employing our method of constraining the effective learning rate, we successfully train the network to achieve an even lower perplexity than that achieved with warm-up, without using any warm-up.

5 Discussion, Limitations and Future Work

Despite its simplicity, our model accurately predicts the qualitative behavior of ELR mean and standard deviation throughout real training using various learning rates. Our findings suggest that the effects captured by our model, though occurring in the initial training phase, significantly influence the entire training process. Additionally, our model predicts that warm-up phases, residual connections and momentum contribute to reducing ELR spread, a prediction we have empirically verified. Notably, our experiments reveal a strong correlation between high ELR spread and low training accuracy. Our results suggest that the effectiveness of warm-up and momentum can at least partly be attributed to lowering ELR spreads.

While our experiments consistently show significant improvements when addressing notably large ELR spreads (e.g. Figure 8 right), we do not claim that merely constraining the ELR suffices in achieving the performance enhancements offered by residual connections, momentum or warm-up or that it is the only effect at play, particularly in the case of more challenging datasets (see Figure 9). Integrating constrained ELR training in a momentum-like setting (eg. Adam, which is known to train better for Transformer architectures) is non-trivial and would constitute an promising line of future research.

References

- Christian H. X. Ali Mehmeti-Göpel, David Hartmann, and Michael Wand. Ringing relus: Harmonic distortion analysis of nonlinear feedforward networks. In *9th International Conference on Learning Representations, ICLR 2021, Virtual Event, Austria, May 3-7, 2021*. OpenReview.net, 2021. URL <https://openreview.net/forum?id=TaYhv-q1Xit>.
- Sanjeev Arora, Zhiyuan Li, and Kaifeng Lyu. Theoretical analysis of auto rate-tuning by batch normalization. In *7th International Conference on Learning Representations, ICLR 2019, New Orleans, LA, USA, May 6-9, 2019*. OpenReview.net, 2019. URL <https://openreview.net/forum?id=rkxQ-nA9FX>.
- Muhammad Awais, Md. Tauhid Bin Iqbal, and Sung-Ho Bae. Revisiting internal covariate shift for batch normalization. *IEEE Trans. Neural Networks Learn. Syst.*, 32(11):5082–5092, 2021. doi: 10.1109/TNNLS.2020.3026784. URL <https://doi.org/10.1109/TNNLS.2020.3026784>.
- David Balduzzi, Marcus Frean, Lennox Leary, J. P. Lewis, Kurt Wan-Duo Ma, and Brian McWilliams. The shattered gradients problem: If resnets are the answer, then what is the question? In Doina Precup and Yee Whye Teh, editors, *Proceedings of the 34th International Conference on Machine Learning, ICML 2017, Sydney, NSW, Australia, 6-11 August 2017*, volume 70 of *Proceedings of Machine Learning Research*, pages 342–350. PMLR, 2017. URL <http://proceedings.mlr.press/v70/balduzzi17b.html>.
- Peter L. Bartlett, Nick Harvey, Christopher Liaw, and Abbas Mehrabian. Nearly-tight vc-dimension and pseudodimension bounds for piecewise linear neural networks. *J. Mach. Learn. Res.*, 20: 63:1–63:17, 2019. URL <http://jmlr.org/papers/v20/17-612.html>.
- Johan Bjorck, Carla P. Gomes, Bart Selman, and Kilian Q. Weinberger. Understanding batch normalization. In Samy Bengio, Hanna M. Wallach, Hugo Larochelle, Kristen Grauman, Nicolò Cesa-Bianchi, and Roman Garnett, editors, *Advances in Neural Information Processing Systems 31: Annual Conference on Neural Information Processing Systems 2018, NeurIPS 2018, December 3-8, 2018, Montréal, Canada*, pages 7705–7716, 2018. URL <https://proceedings.neurips.cc/paper/2018/hash/36072923bfc3cf47745d704feb489480-Abstract.html>.
- Aleksandar Botev, Guy Lever, and David Barber. Nesterov’s accelerated gradient and momentum as approximations to regularised update descent. In *2017 International Joint Conference on Neural Networks, IJCNN 2017, Anchorage, AK, USA, May 14-19, 2017*, pages 1899–1903. IEEE, 2017. doi: 10.1109/IJCNN.2017.7966082. URL <https://doi.org/10.1109/IJCNN.2017.7966082>.
- Luke Nicholas Darlow, Elliot J. Crowley, Antreas Antoniou, and Amos J. Storkey. CINIC-10 is not imagenet or CIFAR-10. *CoRR*, abs/1810.03505, 2018. URL <http://arxiv.org/abs/1810.03505>.
- Jia Deng, Wei Dong, Richard Socher, Li-Jia Li, Kai Li, and Li Fei-Fei. Imagenet: A large-scale hierarchical image database. In *2009 IEEE Computer Society Conference on Computer Vision and Pattern Recognition (CVPR 2009), 20-25 June 2009, Miami, Florida, USA*, pages 248–255. IEEE Computer Society, 2009. doi: 10.1109/CVPR.2009.5206848. URL <https://doi.org/10.1109/CVPR.2009.5206848>.
- Desmond Elliott, Stella Frank, Khalil Sima’an, and Lucia Specia. Multi30k: Multilingual english-german image descriptions. In *Proceedings of the 5th Workshop on Vision and Language, hosted by the 54th Annual Meeting of the Association for Computational Linguistics, VL@ACL 2016, August 12, Berlin, Germany*. The Association for Computer Linguistics, 2016. doi: 10.18653/v1/w16-3210. URL <https://doi.org/10.18653/v1/w16-3210>.
- Moein Hasani and Hassan Khotanlou. An empirical study on position of the batch normalization layer in convolutional neural networks. In *2019 5th Iranian Conference on Signal Processing and Intelligent Systems (ICSPIS)*, pages 1–4, 2019. doi: 10.1109/ICSPIS48872.2019.9066113.
- Kaiming He, Xiangyu Zhang, Shaoqing Ren, and Jian Sun. Delving deep into rectifiers: Surpassing human-level performance on imagenet classification. In *2015 IEEE International Conference on Computer Vision, ICCV 2015, Santiago, Chile, December 7-13, 2015*, pages 1026–1034. IEEE

- Computer Society, 2015. doi: 10.1109/ICCV.2015.123. URL <https://doi.org/10.1109/ICCV.2015.123>.
- Kaiming He, Xiangyu Zhang, Shaoqing Ren, and Jian Sun. Deep residual learning for image recognition. In *2016 IEEE Conference on Computer Vision and Pattern Recognition, CVPR 2016, Las Vegas, NV, USA, June 27-30, 2016*, pages 770–778. IEEE Computer Society, 2016a. doi: 10.1109/CVPR.2016.90. URL <https://doi.org/10.1109/CVPR.2016.90>.
- Kaiming He, Xiangyu Zhang, Shaoqing Ren, and Jian Sun. Identity mappings in deep residual networks. In Bastian Leibe, Jiri Matas, Nicu Sebe, and Max Welling, editors, *Computer Vision - ECCV 2016 - 14th European Conference, Amsterdam, The Netherlands, October 11-14, 2016, Proceedings, Part IV*, volume 9908 of *Lecture Notes in Computer Science*, pages 630–645. Springer, 2016b. doi: 10.1007/978-3-319-46493-0_38.
- S. Hochreiter. Untersuchungen zu dynamischen neuronalen netzen. Diploma thesis, TU Munich, 1991.
- Elad Hoffer, Ron Banner, Itay Golan, and Daniel Soudry. Norm matters: efficient and accurate normalization schemes in deep networks. In Samy Bengio, Hanna M. Wallach, Hugo Larochelle, Kristen Grauman, Nicolò Cesa-Bianchi, and Roman Garnett, editors, *Advances in Neural Information Processing Systems 31: Annual Conference on Neural Information Processing Systems 2018, NeurIPS 2018, December 3-8, 2018, Montréal, Canada*, pages 2164–2174, 2018. URL <https://proceedings.neurips.cc/paper/2018/hash/a0160709701140704575d499c997b6ca-Abstract.html>.
- Sergey Ioffe and Christian Szegedy. Batch normalization: Accelerating deep network training by reducing internal covariate shift. In Francis R. Bach and David M. Blei, editors, *Proceedings of the 32nd International Conference on Machine Learning, ICML 2015, Lille, France, 6-11 July 2015*, volume 37 of *JMLR Workshop and Conference Proceedings*, pages 448–456. JMLR.org, 2015.
- Alex Krizhevsky. Learning multiple layers of features from tiny images. pages 32–33, 2009. URL <https://www.cs.toronto.edu/~kriz/learning-features-2009-TR.pdf>.
- Alex Krizhevsky, Ilya Sutskever, and Geoffrey E. Hinton. Imagenet classification with deep convolutional neural networks. In Peter L. Bartlett, Fernando C. N. Pereira, Christopher J. C. Burges, Léon Bottou, and Kilian Q. Weinberger, editors, *Advances in Neural Information Processing Systems 25: 26th Annual Conference on Neural Information Processing Systems 2012. Proceedings of a meeting held December 3-6, 2012, Lake Tahoe, Nevada, United States*, pages 1106–1114, 2012. URL <https://proceedings.neurips.cc/paper/2012/hash/c399862d3b9d6b76c8436e924a68c45b-Abstract.html>.
- Ekdeep Singh Lubana, Robert P. Dick, and Hidenori Tanaka. Beyond batchnorm: Towards a unified understanding of normalization in deep learning. In Marc’Aurelio Ranzato, Alina Beygelzimer, Yann N. Dauphin, Percy Liang, and Jennifer Wortman Vaughan, editors, *Advances in Neural Information Processing Systems 34: Annual Conference on Neural Information Processing Systems 2021, NeurIPS 2021, December 6-14, 2021, virtual*, pages 4778–4791, 2021. URL <https://proceedings.neurips.cc/paper/2021/hash/2578eb9cdf020730f77793e8b58e165a-Abstract.html>.
- Kyle Luther. Why batch norm causes exploding gradients. Blog post, 2020. URL <https://kyleluther.github.io/2020/02/18/batchnorm-exploding-gradients.html>.
- Kaifeng Lyu, Zhiyuan Li, and Sanjeev Arora. Understanding the generalization benefit of normalization layers: Sharpness reduction. *CoRR*, abs/2206.07085, 2022. doi: 10.48550/arXiv.2206.07085. URL <https://doi.org/10.48550/arXiv.2206.07085>.
- OpenAI. GPT-4 technical report. *CoRR*, abs/2303.08774, 2023. doi: 10.48550/arXiv.2303.08774. URL <https://doi.org/10.48550/arXiv.2303.08774>.
- B.T. Polyak. Some methods of speeding up the convergence of iteration methods. *USSR Computational Mathematics and Mathematical Physics*, 4(5):1–17, 1964. ISSN 0041-5553. doi: [https://doi.org/10.1016/0041-5553\(64\)90137-5](https://doi.org/10.1016/0041-5553(64)90137-5). URL <https://www.sciencedirect.com/science/article/pii/0041555364901375>.

- Tim Salimans and Diederik P. Kingma. Weight normalization: A simple reparameterization to accelerate training of deep neural networks. In Daniel D. Lee, Masashi Sugiyama, Ulrike von Luxburg, Isabelle Guyon, and Roman Garnett, editors, *Advances in Neural Information Processing Systems 29: Annual Conference on Neural Information Processing Systems 2016, December 5-10, 2016, Barcelona, Spain*, page 901, 2016. URL <https://proceedings.neurips.cc/paper/2016/hash/ed265bc903a5a097f61d3ec064d96d2e-Abstract.html>.
- Shibani Santurkar, Dimitris Tsipras, Andrew Ilyas, and Aleksander Madry. How does batch normalization help optimization? In Samy Bengio, Hanna M. Wallach, Hugo Larochelle, Kristen Grauman, Nicolò Cesa-Bianchi, and Roman Garnett, editors, *Advances in Neural Information Processing Systems 31: Annual Conference on Neural Information Processing Systems 2018, NeurIPS 2018, December 3-8, 2018, Montréal, Canada*, pages 2488–2498, 2018. URL <https://proceedings.neurips.cc/paper/2018/hash/905056c1ac1dad141560467e0a99e1cf-Abstract.html>.
- Sam Shleifer, Jason Weston, and Myle Ott. Normformer: Improved transformer pretraining with extra normalization. *CoRR*, abs/2110.09456, 2021. URL <https://arxiv.org/abs/2110.09456>.
- Karen Simonyan and Andrew Zisserman. Very deep convolutional networks for large-scale image recognition. In Yoshua Bengio and Yann LeCun, editors, *3rd International Conference on Learning Representations, ICLR 2015, San Diego, CA, USA, May 7-9, 2015, Conference Track Proceedings*, 2015. URL <http://arxiv.org/abs/1409.1556>.
- Mingxing Tan and Quoc V. Le. Efficientnet: Rethinking model scaling for convolutional neural networks. In Kamalika Chaudhuri and Ruslan Salakhutdinov, editors, *Proceedings of the 36th International Conference on Machine Learning, ICML 2019, 9-15 June 2019, Long Beach, California, USA*, volume 97 of *Proceedings of Machine Learning Research*, pages 6105–6114. PMLR, 2019. URL <http://proceedings.mlr.press/v97/tan19a.html>.
- Ashish Vaswani, Noam Shazeer, Niki Parmar, Jakob Uszkoreit, Llion Jones, Aidan N. Gomez, Lukasz Kaiser, and Illia Polosukhin. Attention is all you need. In Isabelle Guyon, Ulrike von Luxburg, Samy Bengio, Hanna M. Wallach, Rob Fergus, S. V. N. Vishwanathan, and Roman Garnett, editors, *Advances in Neural Information Processing Systems 30: Annual Conference on Neural Information Processing Systems 2017, December 4-9, 2017, Long Beach, CA, USA*, pages 5998–6008, 2017. URL <https://proceedings.neurips.cc/paper/2017/hash/3f5ee243547dee91fbd053c1c4a845aa-Abstract.html>.
- Ashish Vaswani, Samy Bengio, Eugene Brevdo, François Chollet, Aidan N. Gomez, Stephan Gouws, Llion Jones, Lukasz Kaiser, Nal Kalchbrenner, Niki Parmar, Ryan Sepassi, Noam Shazeer, and Jakob Uszkoreit. Tensor2tensor for neural machine translation. In Colin Cherry and Graham Neubig, editors, *Proceedings of the 13th Conference of the Association for Machine Translation in the Americas, AMTA 2018, Boston, MA, USA, March 17-21, 2018 - Volume 1: Research Papers*, pages 193–199. Association for Machine Translation in the Americas, 2018. URL <https://aclanthology.org/W18-1819/>.
- Xiaoxia Wu, Rachel Ward, and Léon Bottou. Wngrad: Learn the learning rate in gradient descent. *CoRR*, abs/1803.02865, 2018. URL <http://arxiv.org/abs/1803.02865>.
- Ruibin Xiong, Yunchang Yang, Di He, Kai Zheng, Shuxin Zheng, Chen Xing, Huishuai Zhang, Yanyan Lan, Liwei Wang, and Tie-Yan Liu. On layer normalization in the transformer architecture. In *Proceedings of the 37th International Conference on Machine Learning, ICML 2020, 13-18 July 2020, Virtual Event*, volume 119 of *Proceedings of Machine Learning Research*, pages 10524–10533. PMLR, 2020. URL <http://proceedings.mlr.press/v119/xiong20b.html>.
- Greg Yang, Jeffrey Pennington, Vinay Rao, Jascha Sohl-Dickstein, and Samuel S. Schoenholz. A mean field theory of batch normalization. In *7th International Conference on Learning Representations, ICLR 2019, New Orleans, LA, USA, May 6-9, 2019*. OpenReview.net, 2019a. URL <https://openreview.net/forum?id=SyMDXnCcF7>.
- Greg Yang, Jeffrey Pennington, Vinay Rao, Jascha Sohl-Dickstein, and Samuel S. Schoenholz. A mean field theory of batch normalization. In *7th International Conference on Learning Representations, ICLR 2019, New Orleans, LA, USA, May 6-9, 2019*. OpenReview.net, 2019b. URL <https://openreview.net/forum?id=SyMDXnCcF7>.

Hongyi Zhang, Yann N. Dauphin, and Tengyu Ma. Fixup initialization: Residual learning without normalization. In *7th International Conference on Learning Representations, ICLR 2019, New Orleans, LA, USA, May 6-9, 2019*. OpenReview.net, 2019. URL <https://openreview.net/forum?id=H1gsz30cKX>.

A Derivations

In this appendix, we expand upon some of the derivations in the main paper.

We start by a brief recap of the notation from the paper. Unless noted otherwise, our model considers simple feed-forward networks organized in L subsequent layers (more complex architectures such as ResNets are modeled by composing such feed-forward blocks in the main paper). Each layer $f^{(\ell)} : \mathbb{R}^{n_{\ell-1}} \rightarrow \mathbb{R}^{n_\ell}$ consists of a linear map with weights W_ℓ , followed by a nonlinearity φ , which might be preceded by a normalization operation.

When obvious from context or irrelevant to the analysis, we will drop the layer index ℓ .

The full network is denoted by $f = f_L \circ \dots \circ f_1$. We assume that we are training the network to minimize an objective functional

$$L(W) = \mathbb{E}_{(\mathbf{x}, \mathbf{y}) \sim p(\mathbf{x}, \mathbf{y})} \ell(f(\mathbf{x}), \mathbf{y}) \approx \sum_{i=1}^n \ell(f(\mathbf{x}_i), \mathbf{y}_i) =: \tilde{L}(W) \quad (15)$$

where ℓ denotes a per-sample loss function such as a categorical cross-entropy loss, least-squares loss, or the similar. The tuples $(\mathbf{x}_i, \mathbf{y}_i)$, $i = 1 \dots n$ refer to the training data, sampled i.i.d. from a data distribution $p(\mathbf{x}, \mathbf{y})$. When using stochastic gradient descent, this refers to a batch, i.e., a subsample of the overall training data. Our arguments hold for both full-batch and stochastic gradient descent as the form/meaning of the loss function does not affect normalization dynamics.

Optimization is done by (stochastic) gradient descent

$$W(t + \lambda) = W_t - \lambda \nabla_W \tilde{L}(W(t)) \quad (16)$$

with learning rate λ . Note that this notation uses a continuous parameter t for the optimization time, but it is only advanced in fixed steps λ , i.e., the value of the weights at the k -th discrete optimization step is denoted by $W(k\lambda)$. This notation simplifies switching between continuous gradient flow and discrete gradient descent.

Weights and gradients are random variables. We characterize the (expected) magnitude of weights at time t by the standard deviation of the norm, i.e., $\sigma(\|W(t)\|)$. As we perform derivations using variances, we use the short-hand notation of $\sigma_w^2(t)$ for the variance at time t .

A.1 Time-Stepping Constraints and Stability

First, we explain more in detail how to obtain constraints on the step sizes for the ODE described in Eq. 6:

$$\frac{\partial}{\partial t} \sigma_w^2(t) = \frac{\lambda c^2}{\sigma_w^2(t)} \quad (17)$$

where $c := \|\nabla_W \tilde{L}(W(0))\| \in O(\alpha^{L-\ell})$ is the magnitude of the initial gradient, assumed to be constant during early training.

In order to study permissible time stepping, we can first bring this equation into canonical form

$$y'(t) = F(y(t)), \quad F(y) = \frac{\lambda c^2}{y} \quad (18)$$

We then compute the derivative of the right-hand side F , in order to linearize the equation for a stability analysis:

$$\frac{dF(y)}{dy} = -\frac{\lambda c^2}{y^2} \quad (19)$$

We can now write F in linearized form

$$F(y_0 + \Delta y) \doteq a \cdot \Delta y + b = -\frac{\lambda c^2}{y_0^2} \Delta y + \frac{\lambda c^2}{y_0} \quad (20)$$

The coefficient

$$a = -\frac{\lambda c^2}{y(t)^2} \tag{21}$$

indicates the sensitivity of the ODE, which is, in particular, related to the stability when solving it numerically. Stability theory tells us that the Euler integrator, which corresponds to naive gradient (stochastic) descent on the gradient flow, is stable when

$$|1 + \lambda a| \leq 1 \tag{22}$$

In other words, resubstituting $y = \sigma_w^2(t)$, we need to ensure that

$$\left| 1 - \lambda \cdot \frac{\lambda c^2}{(\sigma_w(t)^2)^2} \right| \leq 1, \tag{23}$$

i.e.,

$$\frac{\lambda^2 c^2}{\sigma_w(t)^4} \leq 2, \tag{24}$$

and thus

$$\lambda \leq \frac{\sqrt{2} \cdot \sigma_w(t)^2}{c}. \tag{25}$$

Note that, in order to obtain reasonably accurate results, the actually value of λ should be much smaller, maybe 5 – 10% of the maximum value.

At initialization, we have $\sigma_w^2(t) = 2$ and the magnitude c of the initial gradients is exponential in depth. As the stability problems are worst at $t = 0$, due to the $y^2 = \|W(t)\|^4$ in the denominator of a and the monotonously increasing solutions for $\|W(t)\|$ with t , condition (26) is most restrictive at the start of the optimization, i.e., at $t = 0$:

$$\lambda \ll 2\sqrt{2} \cdot \alpha^{-L} \tag{26}$$

Remark: Strictly speaking, stability theory considers the case of ODEs that converge to a finite value and determines divergent behavior in those cases. In our case, $W(t) \in \Theta(\sqrt{t})$ and thus $\lim_{t \rightarrow \infty} W(t) = \infty$. The key insight is, however, that the initial gradient is largest and doing a finite step at this gradient overshoots, which leads to exhaustive dampening due to BatchNorm scaling by an expected σ_w^{-1} . That later steps do not actually converge, due to the non-linear nature of Eq. 6, does not diminish the problem.

Convergence time outside model scope: For constant λ , the resulting estimates for the number of time steps needed to equalize a deeper network are very large, exceeding by far the initial few training steps for which our model assumptions (constant magnitude of the original gradients of the loss function, disregarding BatchNorm) could plausibly hold. For example, in a 50-layer network, we obtain $\lambda \ll 3 \cdot 10^{-5}$ and 100 layers shrink λ below $2.5 \cdot 10^{-9}$.

Warm-up: A viable strategy for convergence, however, is warm-up: The requirement is that we take step sizes smaller than $O(\sigma_w^2(t))$. If, in each step, we take a constant fraction of that bound, $\sigma_w^2(t)$ will grow exponentially in each step, thereby quickly permitting larger step sizes. Accordingly, convergence times decrease to a realistic $\mathcal{O}(\log \alpha^L) = \mathcal{O}(L)$ steps. *This permits convergence to the solution of the ODE in reasonably short time.*

Our experiments show that carefully parametrized warm-up can equalize effective learning rates; our model can thus explain (at least wrt. the aspects considered here) the practical success of the technique.

A.2 Derivation of the Momentum Formula

Please note: The equations presented in Section 4.3 of the main paper were derived from an earlier version where the time variable was parametrized differently and indexing starts at 1. This has been rectified here, and the correct derivations are provided.

In this section, we show the derivation of the equations given in Section 4.3. We consider basic training dynamics following the momentum formula; for simplicity of notation, we consider time

step $t = k\lambda$ and denote $g_k := \nabla W(\lambda k)$, $\widehat{g}_k := \nabla \widehat{W}(\lambda k)$ and $w_k := W(\lambda k)$, where ∇W is the momentum buffer and $\nabla \widehat{W}$ is the "real gradient", before applying the momentum formula but including auto-rate tuning effects.

First, similarly to Equation 4, the current gradient magnitude before applying momentum should be inversely proportional to the current layer weights:

$$\|\widehat{g}_k\|_F = \frac{c}{\|w_k\|_F}. \quad (27)$$

Secondly, the momentum formula from Equation 11 yields:

$$\begin{aligned} g_k &= \mu g_{k-1} + \widehat{g}_k \\ &= \sum_{i=0}^k \mu^{k-i} \widehat{g}_i. \end{aligned} \quad (28)$$

Assuming all \widehat{g}_i are pairwise orthogonal for all $i \in \{0 \dots k\}$, we can use the Pythagorean theorem and obtain:

$$\|g_k\|_F^2 = \sum_{i=0}^k \mu^{2(k-i)} \|\widehat{g}_i\|_F^2. \quad (29)$$

Finally, we unroll the basic SGD update rule in a similar fashion and substitute Equation 28:

$$\begin{aligned} w_{k+1} &= w_k - \lambda g_k \\ &= w_0 - \lambda \sum_{i=0}^k g_i \\ &= w_0 - \lambda \sum_{i=0}^k \sum_{j=0}^i \mu^{i-j} \widehat{g}_j \end{aligned} \quad (30)$$

By rearranging the terms, we can sum all entries for a fixed j with a geometric sum and obtain:

$$w_{k+1} = w_0 - \lambda \sum_{j=0}^k \widehat{g}_j \cdot \frac{1 - \mu^{k+1-j}}{1 - \mu}. \quad (31)$$

By additionally assuming that w_0 and \widehat{g}_i are orthogonal for all $i \in \{0 \dots n\}$, we obtain:

$$\begin{aligned} \|w_{k+1}\|_F^2 &= \|w_0\|_F^2 + \lambda^2 \cdot \sum_{j=0}^k \|\widehat{g}_j\|_F^2 \cdot \left(\frac{1 - \mu^{k+1-j}}{1 - \mu} \right)^2 \\ &= \|w_0\|_F^2 + \lambda^2 \left(\|\widehat{g}_k\|_F^2 + \sum_{j=0}^{k-1} \left(\frac{1 - \mu^{k+1-j}}{1 - \mu} \right)^2 \cdot \|\widehat{g}_j\|_F^2 \right) \end{aligned} \quad (32)$$

In order to compute the evolution of the weight and gradient norms, after initialization of the initial values w_0 and $g_0 = \widehat{g}_0$, one should follow the following steps in a loop:

1. Compute the squared gradient norm $\|\widehat{g}_i\|_F^2$ using Equation 27.
2. Compute the squared momentum buffer norm $\|g_i\|_F^2$ using Equation 29.
3. Compute the squared weight norms $\|w_i\|_F^2$ using Equation 32.

In order to obtain model predictions with momentum, we run the simulation outlined above, storing the history of previous weight norms in a table.

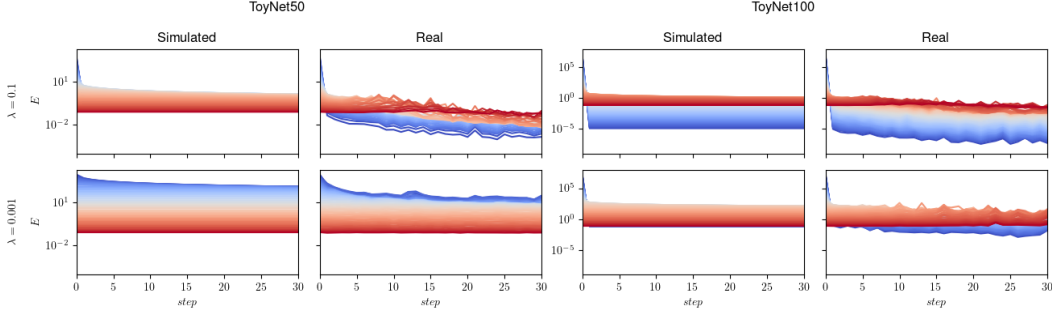


Figure 10: Effective learning rates of the discrete model fitted to the first weight/gradient norm of a ToyNet with 50 and 100 layers, training on Cifar10 compared to the real values measured. We look at two runs with a constant learning rate as indicated.

A.3 Asymptotic Behavior of Gradient Ratios

Since we are interested on the action of auto-rate tuning on the exploding gradient effect, we are interested in the evolution of gradient norm ratios over time. Given two layers ℓ and k that we assume to be the same width with very different initial gradient norms due to exploding gradients at initialization. Using the formula in Section 3.3 for the initial gradient in feedforward networks, it follows from Equation 6 and 7 that:

$$\mathbb{E} \left(\frac{\|\nabla W_\ell\|_F^2}{\|\nabla W_k\|_F^2} \right) (t) = \frac{\lambda c_\ell^2}{\sqrt{2\lambda c_\ell^2 t + k_0}} \cdot \frac{\sqrt{2\lambda c_k^2 t + k_0}}{\lambda c_k^2} \xrightarrow{t \rightarrow \infty} \sqrt{\frac{c_\ell}{c_k}}, \quad (33)$$

which is in most cases a significant reduction from its initial value:

$$\mathbb{E} \left(\frac{\|\nabla W_\ell\|_F^2}{\|\nabla W_k\|_F^2} \right) (0) = \sqrt{\frac{2\lambda c_\ell^2 t + k_0}{2\lambda c_k^2 t + k_0}} \approx \mathcal{O} \left(\frac{c_\ell}{c_k} \right). \quad (34)$$

Using this estimate for the initial base gradient value c , the squared gradient ratio between two layers ℓ and k is reduced asymptotically by a factor $\mathcal{O} \left(\alpha^{\frac{|\ell-k|}{2}} \right)$ in the continuous model.

B Complementary Experiments and Simulations

B.1 Sanity-Checking Our Model

In order to evaluate the goodness of our model, we track the weight and gradient norms of all layers in the first 30 steps of training a very simple ToyNet (ref. Section C) with 50 / 100 layers on Cifar10 for two different constant learning rates, averaged over 20 runs. We fit our discrete model to the initial values for weight and gradient norms (before applying any training step) and extrapolate the remaining steps. We then compute the effective learning rate for the first 30 steps in the discrete model, as well as for the real measurements. In Figure 10 we see that qualitatively, our prediction holds. For the ToyNet50 we see that for the low learning rate, ELRs slowly converge as predicted and for the high learning rate, effective learning rates "flip" at the first step. As for ToyNet100, for the high learning rate, as predicted, the bottom layers flip well below the top layers in the first step and for the low learning rate, the bottom layers flip approximately to the level of the top layers.

We also clearly see the limitation of our model: as our derivation makes the simplifying assumption of constant gradient magnitudes, we would expect deviations in the actual behavior after the first few initial optimization steps. This is the case in these examples: Clearly the gradient magnitude is not

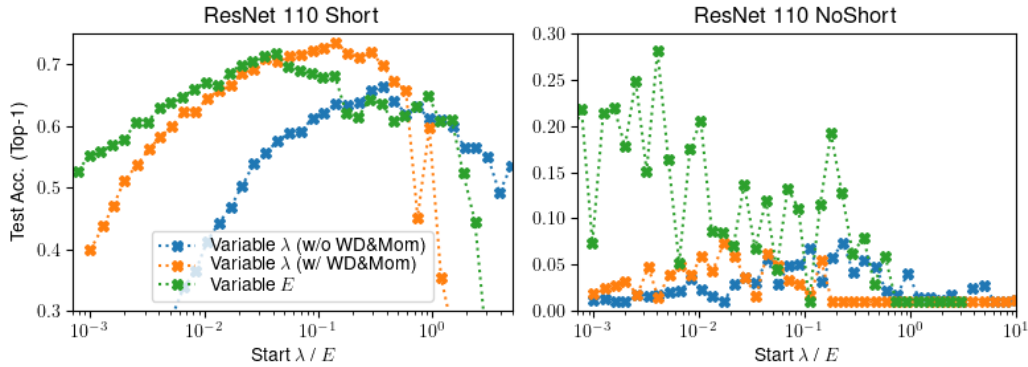


Figure 11: Test accuracy of a ResNet110 Short/NoShort trained on Cifar100 for different initial λ (regular training) or E (constrained ELR training). The dashed line indicates the top accuracy reached.

constant and for the ToyNet50, effective learning rates drop much lower than predicted after only 30 steps. As diametral effects (overshooting and saturation) happen within the first few optimization steps, this limitation of the model is not a strong restriction in the context relevant to this paper. Note that in our model, saturated layers (e.g. lower layers in a ToyNet 100 with $\lambda = 0.1$) can never recover in the future, impacting the entire training process; We verified this empirically, as all measurements of effective learning rates mentioned in the paper are averaged over the entire training process.

B.2 (E)LR Range-Test on Cifar100

We repeat the experiment of Figure 8 to see whether the results still hold on a more difficult dataset. We see in Figure 11 that for the networks with skip-connections the best overall accuracy is reached by the basic training with momentum and weight-decay with 73.6%, followed by constrained ELR training with 71.7% and finally regular training without momentum or weight decay with 66.5%. For the "NoShort" networks, we see that regular training is barely training at all with a top accuracy of 7.3% and training with constrained ELR reaches an accuracy of 28.1%. Overall in the "Short" case, even through constrained ELR training is not able to beat the top accuracy for "Short" networks, its performance is much closer to the orange curve than to the blue curve. For the "NoShort" case, even through the performance of constrained ELR training is not very high, it is significantly higher than the regular training runs that barely train at all. We therefore see our conclusions confirmed.

B.3 Experiments on Transformer Architectures

We want to verify that our ELR constrain method is also applicable to Transformer architectures, we train a Transformer on the Multi30k translation task for our usual three setups, with and without warm-up. We added more LayerNormalization instances to the original Transformer architecture, as discussed in Section C. For this experiment, we did not normalize weight norms at every step since it is more difficult to implement in this setting. In Figure 12 we show the results. First, we note that our SGD baseline generally performs worse than the ADAM baseline. Next, we see that with momentum and weight decay, the model diverges without a initial warm-up phase. Without using SGD or momentum, the full performance is not reached. Using our ELR constrain method, we were able to reach a lower perplexity than the baseline with warm-up, without using any. It seems that with constrained ELR training, we are able to avoid divergence in early training, even without using warm-up.

B.4 Simulations at Different Time Steps

To show that the the results in Figure 4 do not strongly depend on the time step chosen, we show the results of the simulation for different time steps. In Figure 13 see that the effect gets stronger over time: it is weak for 10 steps and strong for 100 time steps but already clearly distinguishable already at 25 time steps.

Optimizer	Constrain	Wd. & Mom.	Warmup	Test Perplexity
ADAM	No	(Yes)	Yes	1.290
SGD	No	Yes	Yes	1.310
SGD	No	Yes	No	Diverged
SGD	No	No	Yes	1.383
SGD	No	No	No	1.385
SGD	Yes	No	No	1.285

Figure 12: Performance of a Transformer architecture on the Multi30k translation task in different settings.

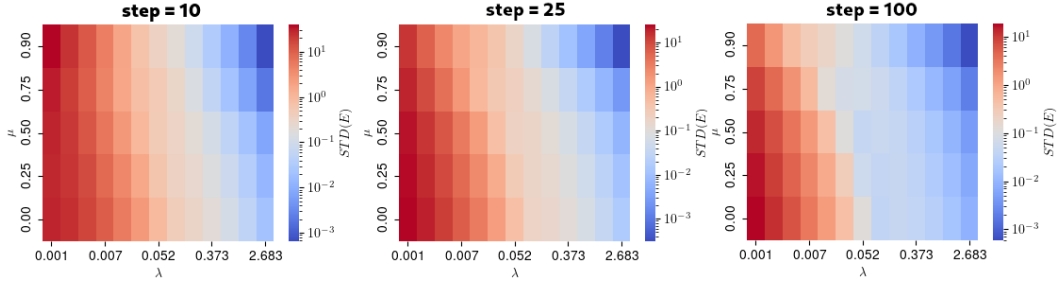


Figure 13: Simulated ELR spread after 10, 25 and 100 steps in our discrete model for different values of λ and μ .

Similarly, we re-run the simulation of Figure 2 for 50 and 100 steps. In Figure 14, we see that qualitatively there is not much difference between the simulations. We conclude that in a setting without momentum, the majority of the shift in effective learning rates happens in the first steps.

C Architecture and Training Details

As described in the main paper, we used ResNet variants with varying hyper-parameters, with and without skip connections. In the appendix, we additionally introduced a very simple ToyNet architecture and a Transformer architecture. Architectural details can be found in the tables below.

ToyNet setup: For comparing direct measurements to our model, we consider a very simple feed-forward convolutional neural network we call *ToyNet* consisting of stacks of Convolutional, Batch-Norm and ReLU layers. All layers have constant width of 32 filters and we use He. initialization so the initial gradient norm of each layer (except the first) is equal; we also exclude the first layer from

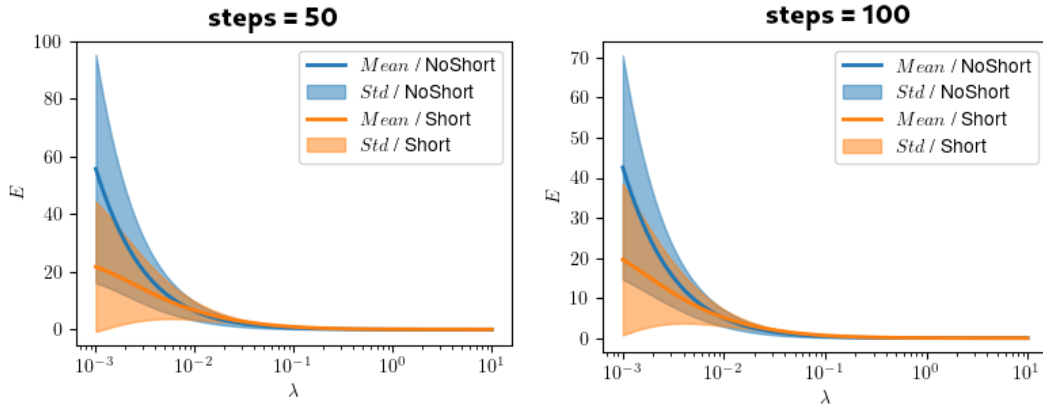


Figure 14: Simulated ELR mean/spread after 50 and 100 steps in our discrete model for different values of λ

Architecture	Transformer	Training	Multi30k
d_{ff}	2048	Epochs	200
d_{model}	512	Scheduler 1	Linear Warmup+Multistep ($\gamma = 0.1$)
h	8	Scheduler 2	Multistep ($\gamma = 0.1$)
N	20	Warmup steps	3000
$p_{dropout}$	0.1	Milestones	160, 180
		Batch size	30
		Gradient Accumulation	10 steps
		Label Smoothing	0.1
		Optimizer 1	ADAM
		ADAM (β_1, β_2)	(0.9, 0.98)
		ADAM Max. LR	0.000806
		ADAM Weight decay	0
		Optimizer 2	SGD
		SGD Max. LR	0.1767
		SGD Momentum	0.9 / 0
		SGD Weight decay	0.0001 / 0
		SGD Nesterov	False

Figure 15: Architecture details and training regime for the NLP task.

Architecture	ResNet110	Architecture	ResNet101 (ImageNet)
Block	BasicBlock v1	Block	BottleneckBlock v1
Num. Blocks	18 18 18	Num. Blocks	3 4 32 3
Num. Planes	16 32 64	Num. Planes	64 128 256 512
Shortcut Type	A (Padding)	Shortcut Type	B (1x1-Conv+BN)

Figure 16: Architecture details for CV tasks.

the plots for this reason. We use BatchNorm without learnable parameters, as initializing with $\beta = 0$ and moving away from the initialization point (the flipping point of ReLU units) reduces the gradient norm additionally. We use a simple SGD optimizer, without weight decay or momentum as they interact with batch-normalization dynamics Lyu et al. [2022]. We use CIFAR-10 as a simple dummy dataset, as we are only interested in the first steps of optimization. We averaged all measurements over 20 different runs. Note that this setup does not train very well or at all and only serves the purpose of validating the predicted effective learning rates of our discrete model.

Modifications on the Transformer architecture: As for the Transformer architecture used in Section B.3, we modified the original transformer architecture by adding more LayerNorm instances to create scale invariance for as many layers as possible. We added a LayerNorm instance after each linear layer in the feedforward block (for a total of 2 in each block) and one additional LayerNorm instance in the attention block after the final multiplication. The latter should give scale-invariance at least to the "value" weights in the attention block. We refrained from adding also a LayerNorm instance to "query" and "key" weights, as this would fundamentally impact the attention mechanism (e.g. attention would not be able to de-saturate anymore in a setting without weight decay); additionally, numerical issues should not arise since SoftMax is bounded, as is its derivative.

The experiments in the paper were made on computers running Arch Linux, Python 3.10.10, PyTorch Version 1.12.0+cu102. Various Nvidia GPUS were used ranging from GeForce GTX 1080TI, GeForce GTX 2080Ti, RTX 4090, Quadro GV100 and A100.

		Training	CINIC-10
Training	CIFAR-10 / CIFAR-100		
Epochs	200	Epochs	50
Scheduler	Multistep ($\gamma = 0.1$)	Scheduler	OneCycle / Cosine
Milestones	100, 150	Max. LR	0.8
Learning rate	Variable	Batch size	256
Batch size	256	Optimizer	SGD + Momentum
Optimizer	SGD + Momentum	Momentum	0.9 / 0
Momentum	0.9 / 0	Nesterov	False
Weight decay	0.0001 / 0	Weight Decay	0.0001 / 0
Augmentation	Random Flip	Augmentation	Random Flip
Nesterov	False	OneCycle AnnealStrategy	Cos
		OneCycle BaseMomentum	0.765
		OneCycle CycleMomentum	True
		OneCycle DivFactor	10
		OneCycle EpochsStart	0.1
		OneCycle FinalDivFactor	1000
		OneCycle MaxMomentum	0.9

Figure 17: Details of the training regime for CIFAR/CINIC computer vision tasks.

Training	ImageNet
Epochs	50
Scheduler	Cosine/OneCycle
Max. LR	0.4
Batch size	100
Optimizer	SGD + Momentum
Nesterov	False
Momentum	0.875
Weight decay	3.051e-05
Augmentation	Random Flip
OneCycle AnnealStrategy	Cos
OneCycle BaseMomentum	0.74375
OneCycle CycleMomentum	True
OneCycle DivFactor	20
OneCycle EpochsStart	0.1
OneCycle FinalDivFactor	2000
OneCycle MaxMomentum	0.875

Figure 18: Details of the training regime for the ImageNet computer vision task.